THE JOURNAL OF PHYSICAL CHEMISTRY C

Article

pubs.acs.org/JPCC

Computational Investigation of DNA Detection Using Single-Electron Transistor-Based Nanopore

Yan-Dong Guo,[†] Xiao-Hong Yan,*[,†,‡] and Yang Xiao[†]

[†]College of Science, Nanjing University of Aeronautics and Astronautics, Nanjing 210016, People's Republic of China

[‡]College of Electronic Science and Engineering, Nanjing University of Posts and Telecommunications, Nanjing 210046, People's Republic of China

Supporting Information

ABSTRACT: We propose a single-electron transistor (SET)-based nanopore sensor for DNA sequencing, which consists of source, drain, and gate electrodes, as well as a nanopore where the DNA molecule is pulled through. For nanopore sensors based on transverse electronic transport, generally, the tunneling current is relatively small due to the weak coupling between the molecule and electrodes. We take full advantage of this feature by introducing SET to make the device operate in Coulomb-blockade regime. Through first-principles simulations, the charge stability diagrams of the nucleobases within the SET-nanopore environment are demonstrated to be distinctive for each molecule and, more importantly, independent of the nucleobase orientation, which can be served as electronic fingerprint for detection. We show that identifying the nucleobases can be achieved only though several specific regions or points in the diagram.

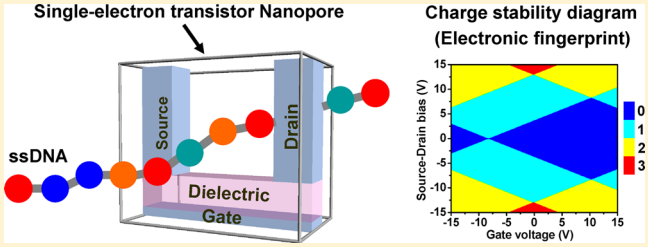

1. INTRODUCTION

The study of DNA sequencing has become a focus of recent research.[1−22] Among them, nanopore (or nanogap) method is considered to be a promising candidate for future DNA sequencing.[23] So far, detection methods based on nanopore have been proposed, e.g., ionic current blockades,[24] optical detection,[25] voltage sensing,[26] and nanopore capacitor.[27] Because of the fast and low-cost features, the sequencing method by measuring the transverse tunneling current of a nanopore when a single-stranded DNA is pulled through it has been widely studied.[1,2,7,10−13,15,20] A nanopore is a small hole connected with electrodes and can be constructed by kinds of materials, e.g., protein, metal, and graphene.[5,15,20,21] Generally, the coupling between molecule and electrodes is not very strong. Moreover, the eigenlevels of the molecule are far away from the Fermi level of electrodes.[20] As a result, the tunneling current is relatively small.[2,4,10,15,20] Many efforts have been devoted to improving the signal strength by increasing the coupling, e.g., Saha et al.[20] and Meunier et al.[4] proposed using nitrogen to passivate the inner side of graphene− or nanoture−nanopore. Here, instead, we take full advantage of the weak coupling feature and explore an alternative idea for DNA sequencing by introducing single-electron transistor (SET) into nanopore, which is inspired by the recent studies that combining the field-effect transistor and nanopore together to improve the sensors.[18,21]

For DNA sequencing devices, weak coupling has its own advantages. First, it can help the molecule to maintain its electronic structure, which is beneficial to detection. Second, the translocation of ssDNA can be realized by small transmembrane bias. Wells et al.[28] studied the translocation dynamics for ssDNA through graphene nanopore. They found that, for the nanopore with small diameter, due to the strong coupling between nanopore and nucleobase, higher transmembrane bias is required to realize the translocation of ssDNA.[28] However, increasing the bias would increase the amount of skips, i.e., the rapid translocation of multiple nucleobases,[28] but smooth translocation can be easily realized by small bias for weaker coupling cases.[28]

For weak coupling system, the electronic transport is incoherent and in the Coulomb-blockade regime. It is the sequential tunneling of single electrons that dominates the transport. In SET-nanopore, not like other biosensors, the molecule is required to weakly couple to electrodes. The transport feature of SET is revealed by its charge stability diagram. Ahmed et al.[17] proposed that, the local density of states (LDOS) of DNA bases, deposited on graphene, can be seen as their electronic fingerprints. In this work, we show that the charge stability diagram is unique and independent of the molecular orientation for each nucleobase within the SET-nanopore, which can also be served as electronic fingerprints for identifying nucleobases.

2. COMPUTATIONAL METHODS

To simulate the operation of SET, Kaasbjerg et al.[29] proposed a semiempirical model. They pointed out the importance of

Received: June 15, 2012
Revised: August 18, 2012
Published: September 19, 2012

polarization-induced renormalization of molecular levels in molecular SET.[29] Stokbro[30] then extended this framework to a description within the density functional theory (DFT), and the calculated charging energies of molecules are in excellent agreement with the experimental results.[30]

In this work, we carry out the simulations by Stokbro's method using the Atomistix ToolKit package.[31,32] The local density approximation (LDA)[33] to the exchange-correlation functional and double-ζ polarized basis set of local numerical orbitals are employed in our calculations. A supercell with sufficient vacuum spaces (more than 10 Å) is chosen to prevent the interactions with adjacent images. The geometries of the molecules are optimized with the Hellman−Feynman forces being smaller than 0.02 eV/Å.

3. RESULTS AND DISCUSSION

By introducing nanopore into SET, we construct a SET-nanopore sensor for DNA sequencing, shown in Figure 1a. It consists of source, drain, and gate electrodes. To form a nanopore, we have enlarged the source and drain electrodes in the traditional SET (Figure 1b). In real application, the single-stranded DNA (ssDNA) will be pulled through this pore by a vertical electric field. When a nucleobase enters into the nanopore, it plays the role of an island in SET for facilitating the electronic transport from source to drain. For SET, the transport feature is revealed by its charge stability diagram. It is this diagram that we will use for the identification of nucleobases. In the following, we will interpret the operating mechanism of our device and show how to obtain that diagram in both theoretical and experimental ways.

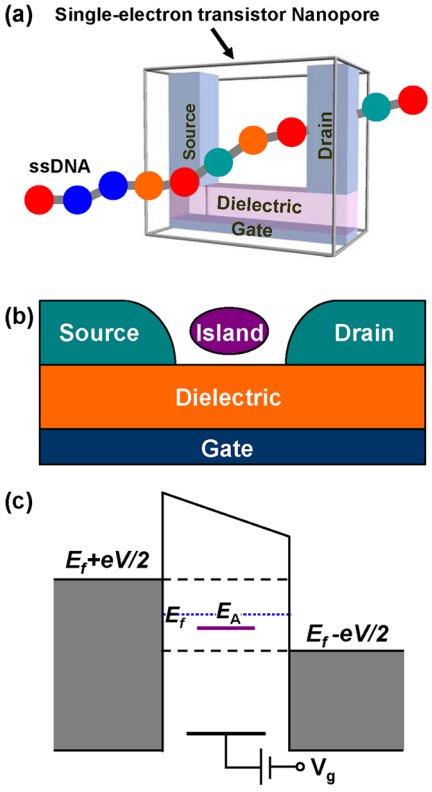

Figure 1. (a) Schematic view of single-electron transistor nanopore. (b) Schematic view of a single-electron transistor. (c) Alignment of molecular electron affinity level (E_A) in the SET environment, which can be shifted by the gate voltage.

The nanopore (or nanogap) sensors constructed by metal electrodes have been studied before.[1,2] Compared with our SET-nanopore, the main difference between them is the electronic transport mechanism. In previous devices, the transport is coherent, but for SET-nanopore, it is incoherent. The key factor, that results in the difference, is the coupling strength between the molecule and electrodes. If the coupling is strong, the molecular electronic levels will be broadened.[30,34] The broaden effect is characterized by the coefficient Γ, which also means that the electrons will stay on the molecule for a short time, $1/\Gamma$. For the electron on molecule, its coherent lifetime is represented by τ_c. If $\tau_c \gg 1/\Gamma$, the electron can transport coherently through the whole system.[30,34] That means, once a scatting state is occupied, it will carry a current from one electrode to another, but if the molecule is weakly coupled to the electrodes, the relationship will be $\tau_c \ll 1/\Gamma$,[30,34] which makes the electron stay on the island for a relatively long time when it tunnels from source to the molecule. As a result, all the information about its previous quantum state will be lost. After that, when it tunnels to the drain, the tunneling process will be independent from the former one (from source to the molecule). This is called sequential tunneling, and apparently, the transport is incoherent. Because of the exclusion principle, Coulomb-blockade will occur in this weak coupling regime, and it is where the SET operates. For molecular device, the distance between molecule and electrodes is essential, as it will affect their coupling strength largely.[13] By choosing longer molecule−electrode distance, we make SET-nanopore operate in a weak coupling regime (Supporting Information).

To obtain the charge stability diagram of SET in theory, we define three functions $E^s(N)$, $E^i(N)$, and $E^d(N)$,[30] which represent the total energies of source, island, and drain with N electrons, respectively. To form a transport from source to drain, the island must have an electronic state within the bias window, shown in Figure 1c. This can be achieved by shifting the positions of molecular levels and electron affinity level through gate voltage (V_g). From the viewpoint of energy, to achieve the transport of an electron from source to the island, the following must be satisfied:

$$E^s(N) + E^i(P) \geq E^s(N-1) + E^i(P+1) \quad (1)$$

where N and P are the initial numbers of electrons on the source and island, respectively. Similarly, the requirement for the process from the island to drain is

$$E^i(P+1) + E^d(Q) \geq E^i(P) + E^d(Q+1) \quad (2)$$

where Q is the initial number of electrons on the drain. Thus, when these two formulas are both satisfied, the electron can move from the source to drain. One thing that should be noted is that this process is incoherent, which means losing or gaining energy may happen during the transport. Taking into account the work function (W) of the metal electrode, the maximum energy of an electron in source is $-W + eV/2$ (the Fermi energy is set to be zero). Similarly, the minimum of an electron in the drain is $-W - eV/2$. So we obtain

$$-W + eV/2 \geq E^s(N) - E^s(N-1) \quad (3)$$

$$E^d(Q+1) - E^d(Q) \geq -W - eV/2 \quad (4)$$

dx.doi.org/10.1021/jp305909p | J. Phys. Chem. C 2012, 116, 21609−21614

Finally, combining all the above formulas, to form the current should satisfy

$$-eV/2 \le E^{i}(P+1) - E^{i}(P) + W \le eV/2 \quad (5)$$

where $\Delta E^{i}(P) = E^{i}(P+1) - E^{i}(P)$ is defined as the charging energy of the island with P electrons.[30]

There are a total of four kinds of DNA bases: adenine (A), cytosine (C), guanine (G), and thymine (T). Here, we take nucleobase A as an example to calculate the charging energies in SET-nanopore environment. The geometry of the molecule in SET-nanopore is illustrated in Figure 2b. The thickness of

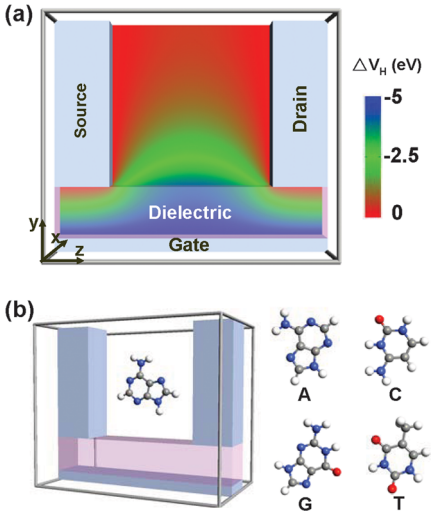

Figure 2. (a) Configuration of SET-nanopore adopted in this article and the contour plot of electrostatic potential under zero source−drain bias and a gate voltage of 5 V. (b) Side view of a nucleobase-embedded SET-nanopore and the molecular structures of nucleobases: adenine (A), cytosine (C), guanine (G), and thymine (T).

the dielectric material is 3.8 Å, with the dielectric constant of $10\varepsilon_0$.[30] The distance between metallic source and drain electrodes is fixed to be 1.2 nm, and the image plane of the metal surface has been taken into account in the electrodes.[30,35] The length of the source and drain electrodes in the y-axis direction is also 1.2 nm. The thickness of the whole device in the x-axis direction is 3.0 Å. We apply the method developed by Stokbro[30] to calculate the charging energies of nucleobases in the SET-nanopore electrostatic environment.

As an example, Figure 3 shows the total energy as s function of V_g with different charge states for nucleobase A in the SET-nanopore environment. Charging energies can be obtained by subtracting them, i.e., $\Delta E(P) = E(P+1) - E(P)$. The reservoir energy of qW is included in the total energy, and q represents the charge of the molecule. We here model the source and drain as Au electrodes with $W = 5.28$ eV, and they can be changed to other metals. As one finds in Figure 3, the negative charge states are more stabilized when $V_g > 0$ (it will be more obvious for larger V_g), and for $V_g < 0$, the positive charge states are more stabilized (it will also be more obvious for smaller V_g). This is in agreement with the shifting of molecular levels by V_g. A negative V_g will push them up, and when the highest occupied molecular orbital (HOMO) is pushed above the Fermi level of the electrode, it will lose an electron and become positively charged. On the contrary, a positive V_g will lower the molecular levels. When the lowest unoccupied molecular orbital (LUMO) is below the Fermi level of the electrode, it will gain

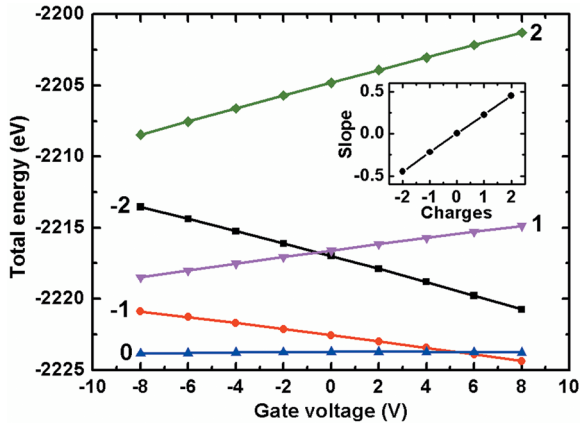

Figure 3. Total energy as a function of gate voltage with different charge states for nucleobase A in the SET-nanopore environment. The inset shows the linearly fitting slopes for different charge states, and they also exhibit good linear behavior against charges.

an electron and become negatively charged. Because of the planar structure of the molecule, the total energy exhibits good linear behavior against V_g.[30] The slopes of linear fitting for each charge state are shown in the inset of Figure 3. The slopes themselves also show good linear behavior against the charge states q, for the planar structure.[30] To investigate this linear dependence further, we fit a linear function for total energy[30]

$$E = E(q)_{V_g=0} + \alpha q V_g \quad (6)$$

with $\alpha = 0.2241$.

With eqs 5 and 6, we can easily get the charge stability diagram for nucleobase A in SET-nanopore, shown in Figure 4 (denoted as A0). For a SET, the charge stability diagram can reveal its transport properties. For a given source-drain bias (V_b) and gate voltage (V_g), the conductance of the device is decided by the number of molecular energy levels inside the bias window. This number is represented by the color code in the charge stability diagram (see Figure 4). By adjusting V_g, the energy level can be shifted in or out of the bias window. As a result, the color diagram is related to both V_b and V_g. As the SET-nanopore device operates in a weak coupling regime, the nucleobase molecule can maintain its molecular electronic structure well. Thus, the charge stability diagram is able to represent the unique feature of each nucleobase.

To obtain the charge stability diagram in experiment, we can perform the measurement according to the following steps. For a given V_g and V_b, the current of SET-nanopore can be measured. If we perform a scan for V_b (with fixed V_g), an $I-V_b$ curve can be obtained. Because of the Coulomb blockage, the current will increase in steps, corresponding to the increase of integer excess electrons on the island.[36] Using dI/dV_b, we can derive the differential conductance, which will exhibit periodic Coulomb oscillations.[36] If one also performs the scan for V_g, then a two-dimensional diagram for differential conductance can be gotten, with V_g and V_b to be the axes. In a gray or color scaled diagram of the conductance, the diamond pattern, like our diagram, will emerge. As in the increase of current, one step corresponds to one electron, the diamonds can be easily numbered by the excess charge on the island.[37] Then, the charge stability diagram is obtained. As the diagram can be measured in experiment,[37] utilizing it for DNA sequencing becomes feasible.

dx.doi.org/10.1021/jp305909p | J. Phys. Chem. C 2012, 116, 21609−21614

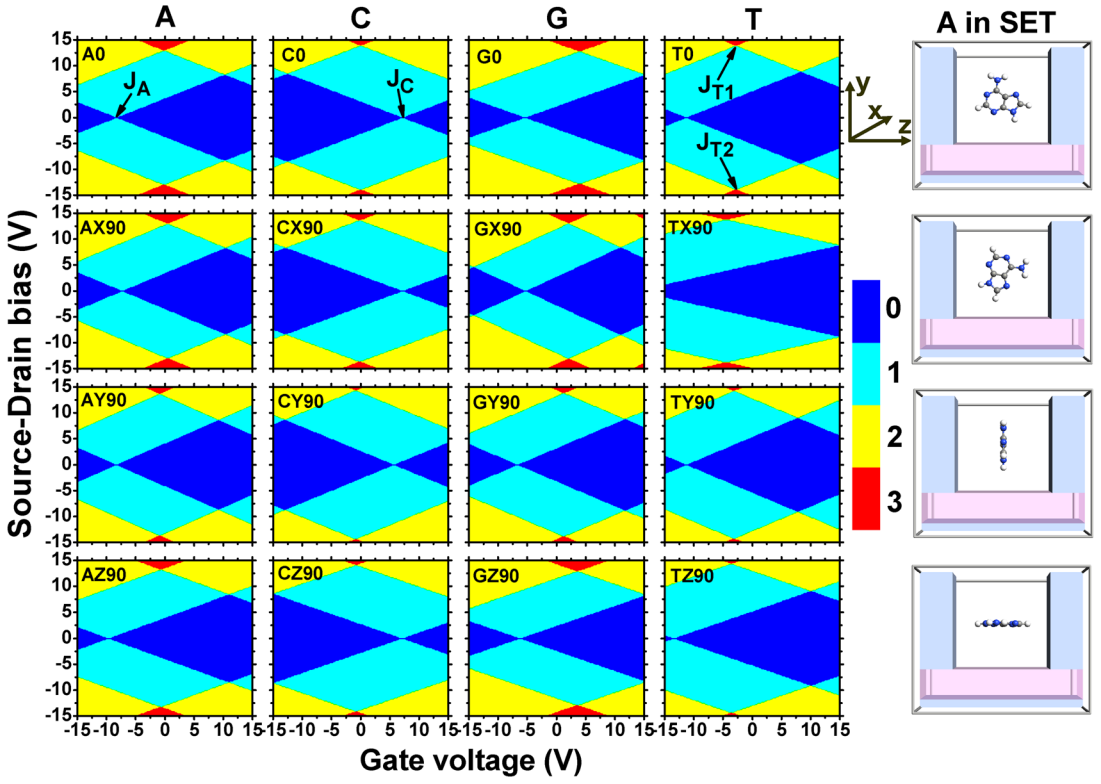

Figure 4. Charge stability diagrams for nucleobases A, C, G, and T in SET-nanopore with different orientations. The right panel shows the corresponding orientation configuration for each row (adenine is chosen as an example). The first row is for nonrotation cases. The second, third, and fourth rows are for rotating the nucleobases by 90° around the *x*-, *y*-, and *z*-axes, respectively (Supporting Information shows the 45°-rotation cases). As an example, "CY90" in the third row means rotating nucleobase C by 90° around the *y*-axis.

Like A0 in Figure 4, the charge stability diagrams for nucleobases C, G, and T within the SET-nanopore can also be obtained, shown in the first row of Figure 4 (denoted as C0, G0, and T0). One finds that, the four diagrams in the first row (A0, C0, G0, and T0) are different from each other. It is easy to identify them through the diagrams. For SET-nanopore, the transport property is mainly determined by the molecular electronic structures. The weak coupling between the molecule and electrodes makes the nucleobase maintain its electronic levels well. So the diagram could represent the intrinsic and unique feature for each nucleobase. In previous studies, Ahmed et al.[17] proposed that the local density of states (LDOS) of DNA bases, deposited on graphene, can be seen as their electronic fingerprints. As our diagrams are two-dimensional ones, actually, they are more like fingerprints.

However, when the DNA strand is pulled through the SET-nanopore, the orientation of the nucleobase is not always like what they are now. We should make sure that the identification can be available for other orientations. Here, we consider three other orientations, i.e., rotating the molecule by 90° around the *x*-, *y*-, and *z*-axes, respectively. The corresponding charge stability diagrams are shown in the second, third, and fourth rows in Figure 4, respectively. As an example for the denotation, "CY90" in the third row means rotating nucleobase C by 90° around the *y*-axis. From the figure, we can see that, for each nucleobase (each column), the color pattern maintains well during the rotation. There are only minor changes in the diagrams for nucleobases A, C, and G during the rotation. As the molecule is weakly coupled to the electrodes, the orientation only induces a minor effect on the molecular electronic structure. For nucleobase T, when it is rotated by 90° around the *x*-axis, the color pattern TX90 (especially the region around zero-bias) undergoes a relatively larger change, compared with T0, TY90, and TZ90. Even so, there are still some specific regions or points in the diagram that remain unchanged. For example, the gate voltages of the 1−2−3 charge-state junction points (denoted as J_{T1} and J_{T2}) are independent of the nucleobase orientation. We can use such specific regions or points instead of the whole diagram to identify the nucleobases, which could speed up the sequencing.

By examining the patterns of other nucleobases in Figure 4, one can find such 1−2−3 charge-state junction points exhibit distinctive variation features in gate voltage for each nucleobase, independent of the molecular orientation. For clarity, the variation of V_g at these junction points for each nucleobase is plotted in Figure 5. That is to say, when the nucleobase orientation changes like adenine in the right penal in Figure 4, the gate voltage of the 1−2−3 charge-state junction points will vary within the V_g intervals in Figure 5. Apparently, for nucleobases G and T, there is no overlap of V_g intervals with each other and no overlap with that of A and C. So, it is easy to identify them from others. As for nucleobases A and C, there is a large overlap V_g region. Even the whole V_g interval of C is in it. It is impossible to identify A and C only by this junction point. Actually, if one looks at the left two columns in Figure 4 again, one will find that the nucleobases A and C are very easy to identify. The diagrams in the first column (A) and in the second column (C) are quite different, especially in the middle region of the diagrams. At the same time, each column can maintain its own color pattern well, independent of the nucleobase orientation. We can choose some other typical regions or points for identification. For instance, the 0−1

dx.doi.org/10.1021/jp305909p | J. Phys. Chem. C 2012, 116, 21609−21614

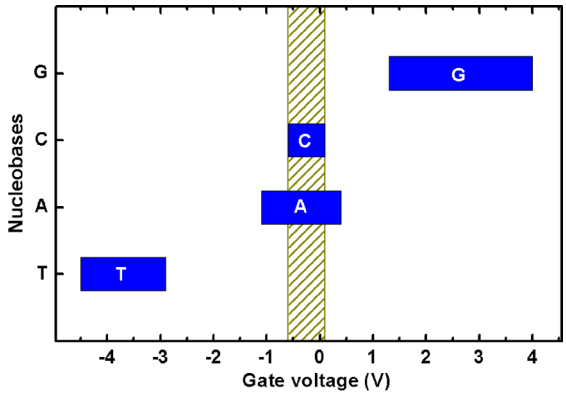

Figure 5. Variation of the gate voltage of the 1−2−3 charge-state junction points (such as J_{T1} and J_{T2} for nucleobase T in Figure 4) due to the rotation of the nucleobase (A, C, G, and T) within SET-nanopore. The shaded rectangle represents the overlap between the V_g intervals for different nucleobases. The specific configurations of the nucleobases in SET-nanopore, which define the V_g intervals, are shown in the right panel of Figure 4.

charge-state junction points (denoted as J_A and J_C) can be chosen to identify nucleobases A and C. In brief, if several specific regions or points in the diagrams are compared, the identification of the four nucleobases can be achieved. Besides, the charge stability diagrams for the cases with rotation angle of 45° are also calculated (Supporting Information). Not surprisingly, they are consistent with the above analysis for the 90° cases. Furthermore, we also calculate the charge stability diagrams of nucleobase A within SET-nanopore for different base positions and find that the change of position (in a finite range) has only a minor effect on the diagrams (Supporting Information). The reason is as follows. Although the nucleobase−electrode distances have been changed, the coupling between them is still weak. According to the operating mechanism of SET-nanopore, in the weak regime, the transport feature and corresponding charge stability diagram is mainly determined by the electronic structure of the nucleobase itself. Therefore, the color pattern of a DNA base in SET-nanopore is able to represent its own intrinsic feature and thus can be served as electronic fingerprint for identification.

In the above simulations, we use Au as the electrode's material. Actually, it can be replaced by other metals, e.g., Ag and Cu. Recently, plenty of works focus on the application of graphene in DNA sequencing.[11−14,16,17,20] The most important advantage of it is the thickness, which can ensure that only one DNA base exists in the nanopore at a time. Wells et al.[28] have investigated the translocation process of ssDNA through graphene nanopore and found that the hydrophobic interaction could induce specific orientations of ssDNA in the nanopore. As graphene-based SET can be fabricated in experiment,[38,39] graphene might be another good candidate for the electrodes in our SET-nanopore, which we will not discuss in the present work.

For practical application, the isolated nucleobases will be assembled by sugar−phosphate backbone, and the device will be immersed into water with electrolyte, where the DNA translocation can be driven by a vertical electric field. There are lots of factors, such as water and ions, which may change the electrostatic field surrounding SET and influence the DNA sequencing. According to previous studies, some might induce tiny influence, e.g., the backbone would only induce an offset for all bases,[1] and water would lower the current by a few percent on average,[2] while some factors may induce huge effect. For each factor, there might be many influencing ways to be considered, e.g., different positions, orientations, and speeds of the ions. Those need a systematic and detailed investigation. In this article, we focus on the fundamental problems of combining SET and nanopore together for DNA sequencing and will explore in more quantitative details in future studies.

For the real device, temperature is an important parameter to be considered. In this work, we have taken it into account by setting the temperature as 300 K in the Fermi function during the calculation.[30] According to former related studies,[13,36,37] a rough estimate of the current of our device at room temperature under V_b = 1.0 V is $\sim 10^{-6}$ nA.

For practical application of the device, fluctuations of current will occur, which mainly come from two parts.[2] The first part is the noise correlated with the current itself, e.g., $1/f$ and thermal noise. It is found that these noises either can be overcome or only induce negligibly small error in the current.[2] Therefore, the second part, structural motions of DNA and environment, are the main source of the fluctuations in the current.[2] For the influence of the environment, as mentioned above, it is important but involves many issues to be considered, which we will explore in future studies. As for the motion of DNA, we have shown that the orientation and position (in a finite range) of the nucleobase have only a minor effect on the charge stability diagrams due to the weak coupling. According to those diagrams, an estimate of the fluctuation of the charge-state junction points used for distinguishing nucleobases is less than 6%, which will not induce the confusion of nucleobases.

4. CONCLUSIONS

Through first-principles simulations, we propose and investigate a single-electron transistor-based nanopore sensor for DNA sequencing, which relies on the transverse electronic transport. The device operates in Coulomb-blockade regime, and the electronic transport is interpreted by sequential tunneling of single electrons. The proposed method takes full advantage of the weak coupling between the molecule and electrodes. In SET-nanopore sensor, the charge stability diagrams of the nucleobases within the SET-nanopore environment are found to be distinctive for each molecule and independent of the nucleobase orientation and positions. As the electronic transport is mainly determined by the molecular electronic structure due to the weak coupling, the diagram could represent the intrinsic feature of the nucleobases and can be served as electronic fingerprint for identification. Furthermore, we demonstrate that several specific regions or points in the diagram are enough to identify the DNA bases.

■ ASSOCIATED CONTENT

Supporting Information

Comparison of geometric structure with previous studies, charge stability diagrams of nucleobase A within SET-nanopore for different electrode−nucleobase distances, total energy as function of V_g for nucleobases within the SET-nanopore, and the charge stability diagrams for 45°-orientation cases. This material is available free of charge via the Internet at http://pubs.acs.org.

■ AUTHOR INFORMATION

Corresponding Author

*E-mail: xhyan@nuaa.edu.cn.

Notes

The authors declare no competing financial interest.

■ ACKNOWLEDGMENTS

This work was supported by the National Natural Science Foundation of China (NSFC10874089 and NSFC51032002), the key project of National High Technology Research and Development Program of China (2011AA050526), the Science and Technology Support Plan of Jiangsu Province (BE2011191), the Funding of Jiangsu Innovation Program for Graduate Education (CXZZ11_0190 and CX08B_005Z), and the Fundamental Research Funds for the Central Universities (NS2012064).

■ REFERENCES

(1) Zwolak, M.; Ventra, M. D. *Nano Lett.* **2005**, *5*, 421−424.
(2) Lagerqvist, J.; Zwolak, M.; Ventra, M. D. *Nano Lett.* **2006**, *6*, 779−782.
(3) He, H.; Scheicher, R. H.; Pandey, R.; Rocha, A. R.; Sanvito, S.; Grigoriev, A.; Ahuja, R.; Karna, S. P. *J. Phys. Chem. C* **2008**, *112*, 3456−3459.
(4) Meunier, V.; Krstić, P. S. *J. Chem. Phys.* **2008**, *128*, 041103.
(5) Zwolak, M. *Rev. Mod. Phys.* **2008**, *80*, 141−165.
(6) Bahrami, M.; Rungger, I.; Sanvito, S. *Nanotechnology* **2010**, *21*, 445501.
(7) Bayley, H. *Nature* **2010**, *467*, 164−165.
(8) Garaj, S.; Hubbard, W.; Reina, A.; Kong, J.; Branton, D.; Golovchenko, J. A. *Nature* **2010**, *467*, 190−193.
(9) He, Y.; Shao, L.; Scheicher, R. H.; Grigoriev, A.; Ahuja, R.; Long, S.; Ji, Z.; Yu, Z.; Liu, M. *Appl. Phys. Lett.* **2010**, *97*, 043701.
(10) Huang, S.; He, J.; Chang, S.; Zhang, P.; Liang, F.; Li, S.; Tuchband, M.; Fuhrmann, A.; Ros, R.; Lindsay, S. *Nat. Nanotechnol.* **2010**, *5*, 868−873.
(11) Merchant, C. A.; Healy, K.; Wanunu, M.; Ray, V.; Peterman, N.; Bartel, J.; Fischbein, M. D.; Venta, K.; Luo, Z.; Johnson, A. T. C. *Nano Lett.* **2010**, *10*, 2915−2921.
(12) Nelson, T.; Zhang, B.; Prezhdo, O. V. *Nano Lett.* **2010**, *10*, 3237−3242.
(13) Postma, H. W. C. *Nano Lett.* **2010**, *10*, 420−425.
(14) Schneider, F.; Kowalczyk, S. W.; Calado, V. E. *Nano Lett.* **2010**, *10*, 3163−3167.
(15) Tsutsui, M.; Taniguchi, M.; Yokota, K.; Kawai, T. *Nat. Nanotechnol.* **2010**, *5*, 286−290.
(16) Min, S. K.; Kim, W. Y.; Cho, Y.; Kim, K. S. *Nat. Nanotechnol.* **2011**, *6*, 162−165.
(17) Ahmed, T.; Kilina, S. V.; Das, T.; Haraldsen, J. T.; Rehr, J. J.; Balatsky, A. V. *Nano Lett.* **2012**, *12*, 927−931.
(18) Anselmetti, D. *Nat. Nanotechnol.* **2012**, *7*, 81−82.
(19) Raillon, C.; Cousin, P.; Traversi, F.; Garcia-Cordero, E.; Hernandez, N.; Radenovic, A. *Nano Lett.* **2012**, *12*, 1157−1164.
(20) Saha, K.; Drndic, M.; Nikolic, B. K. *Nano Lett.* **2012**, *12*, 50−55.
(21) Xie, P.; Xiong, Q.; Fang, Y.; Qing, Q.; Lieber, C. M. *Nat. Nanotechnol.* **2012**, *7*, 119−125.
(22) Iqbal, S. M.; Akin, D.; Bashir, R. *Nat. Nanotechnol.* **2007**, *2*, 243−248.
(23) Branton, D.; Deamer, D. W.; Marziali, A.; Bayley, H.; Benner, S. A.; Butler, T.; Di Ventra, M.; Garaj, S.; Hibbs, A.; Huang, X. *Nat. Biotechnol.* **2008**, *26*, 1146−1153.
(24) Vercoutere, W.; Winters-Hilt, S.; Olsen, H.; Deamer, D.; Haussler, D.; Akeson, M. *Nat. Biotechnol.* **2001**, *19*, 248−252.
(25) McNally, B.; Singer, A.; Yu, Z.; Sun, Y.; Weng, Z.; Meller, A. *Nano Lett.* **2010**, *10*, 2237−2244.
(26) Gracheva, M. E.; Xiong, A.; Aksimentiev, A.; Schulten, K.; Timp, G.; Leburton, J. P. *Nanotechnology* **2006**, *17*, 622.
(27) Sigalov, G.; Comer, J.; Timp, G.; Aksimentiev, A. *Nano Lett.* **2008**, *8*, 56−63.
(28) Wells, D. B.; Belkin, M.; Comer, J.; Aksimentiev, A. *Nano Lett.* **2012**, *12*, 4117−4123.
(29) Kaasbjerg, K.; Flensberg, K. *Nano Lett.* **2008**, *8*, 3809−3814.
(30) Stokbro, K. *J. Phys. Chem. C* **2010**, *114*, 20461−20465.
(31) Brandbyge, M.; Mozos, J.-L.; Ordejón, P.; Taylor, J.; Stokbro, K. *Phys. Rev. B* **2002**, *65*, 165401.
(32) QuantumWise. http://www.quantumwise.com/.
(33) Perdew, J. P.; Zunger, A. *Phys. Rev. B* **1981**, *23*, 5048−5079.
(34) Datta, S. *Electronic Transport in Mesoscopic Systems*; Cambridge University Press: Cambridge, U.K., 1997.
(35) Chulkov, E. V.; Silkin, V. M.; Echenique, P. M. *Surf. Sci.* **1999**, *437*, 330−352.
(36) Matsumoto, K.; Ishii, M.; Segawa, K.; Oka, Y.; Vartanian, B.; Harris, J. *Appl. Phys. Lett.* **1996**, *68*, 34.
(37) Kubatkin, S.; Danilov, A.; Hjort, M.; Stuhr-Hansen, N.; Hedega, P.; Bre, J-I. *Nature* **2003**, *425*, 14−17.
(38) Ihn, T.; Güttinger, J.; Molitor, F.; Schnez, S.; Schurtenberger, E.; Jacobsen, A.; Hellmüller, S.; Frey, T.; Dröscher, S.; Stampfer, C. *Mater. Today* **2010**, *13*, 44−50.
(39) Stampfer, C.; Schurtenberger, E.; Molitor, F.; Guttinger, J.; Ihn, T.; Ensslin, K. *Nano Lett.* **2008**, *8*, 2378−2383.